# Part III:
# Circumstellar Properties of Intermediate-Age PMS Stars

# Chapter 7

# Spitzer Observations of 5 Myr-old Brown Dwarfs in Upper Scorpius

## 7.1 Introduction

Ground-based infrared studies have found that while disks are commonplace around stars in the most recently formed clusters ($\lesssim$1 Myr; Kenyon & Hartmann 1995; Skrutskie et al. 1990), by an age of $\sim$10 Myr, dust is removed from the inner few AU of circumstellar disks for most stars (Mamajek et al., 2004). Since the launch of the *Spitzer Space Telescope* in 2003, studies aiming to probe circumstellar disks have extended to longer wavelengths and hence larger disk radii. Sicilia-Aguilar et al. (2006) used IRAC and MIPS observations to probe inner circumstellar disks from $\sim$0.1 to 20 AU for stars in the $\sim$10 Myr-old NGC 7160 association and found that $<$4% of stars in this region still retain disks at these radii. Silverstone et al. (2006) used IRAC to survey 45 nearby sunlike stars with ages 10–30 Myr and found that only 1/45 stars ($<$3%) had mid-infrared excess emission indicating the presence of an inner disk. Between the ages of $\sim$1 and 10 Myr, stars must be in the process of actively clearing circumstellar material, presumably through a combination of accretion, photoevaporation or planet-formation.

Observational evidence (e.g., Guieu et al. 2007, Allers et al. 2006) has found that even the lowest mass pre-main sequence stars and young brown dwarfs form with a circumstellar disk in a manner analogous to solar-type stars. However, the evolution

of material around such extremely low mass objects may not follow the same path as that for their higher mass stellar counterparts. Disks are heated via a combination of irradiation and accretion. The much lower temperatures and masses of brown dwarfs compared to solar-type pre-main sequence stars may cause differences in the evolution of accretion, disk composition and grain size. The standard photoevaporative model (e.g., Hollenbach et al. 1994) of high mass disk destruction requires a high flux of EUV Lyman continuum photons from a hot central object to ionize and heat the disk surface. In the absence of an outside source of ionizing radiation, the photoevaporative disk destruction rate decreases with decreasing stellar mass due to much lower levels of EUV photons produced, possibly leading to longer disk lifetimes with corresponding effects on the potential of brown dwarfs and low mass stars to form planetary systems.

Rapidly increasing knowledge garnered from *Spitzer* observations has been suggestive that the lifetime of circumstellar disks is, in fact, dependent on the mass of the central object. Carpenter et al. (2006) took IRAC 4.5$\mu$m and 8$\mu$m observations of $\sim$200 stars ranging from $\sim$20 to 0.1 $M_{\odot}$ in the 5 Myr-old USco association. This study found the frequency of stars which still harbored a mid-infrared excess at 5 Myr to be strongly spectral type dependent, with the coolest stars (K-M types) preferentially retaining their inner disks longer than those stars at intermediate temperatures (F-G types). A similar study by Dahm & Hillenbrand (2007) used IRAC observations to explore the 5 Myr-old NGC 2362 association across all stars from spectral type B2 to M5, and found that no star more massive than $\sim$1.2 $M_{\odot}$ exhibited a significant mid-infrared excess short-ward of 8.0$\mu$m. These results are supported by similar findings in the $\sim$3 Myr-old $\sigma$Ori cluster (Hernández et al., 2007), the $\sim$3 Myr-old IC 348 cluster (Lada et al., 2006), the $\sim$5–9 Myr-old $\eta$ Chameleontis association (Megeath et al., 2005), and the 25 Myr-old NGC 2547 cluster (Young et al., 2004).

In this chapter I present a mid-infrared study of brown dwarf members of the 5 Myr-old USco association, thus extending the work by Carpenter et al. (2006) into the substellar regime. I use results from these observations to probe circumstellar disk evolution as a function of mass at 5 Myr, and as a function of age for substellar mass objects.

## 7.2 Observations

I obtained 3.6, 4.5, 5.8, 8.0, and 24 $\mu$m images with IRAC (Fazio et al., 2004) and MIPS (Rieke et al., 2004) cameras on the *Spitzer Space Telescope* for 27 low mass members of USco identified originally from my first set of Palomar spectroscopic observations (Slesnick et al. 2006, hereafter SCH06; see also chapters 2, 3, & 5). The sources in the *Spitzer* sample were selected first as candidate members based on optical/near-infrared colors and magnitudes, and confirmed spectroscopically to have cool temperatures and low surface gravity consistent with low mass USco members. These objects therefore represent an unbiased sample in that they were identified independent of any circumstellar signatures. All targets have spectral type M6–M8, where spectral types M6 and later correspond to substellar masses ($\lesssim$0.08 $M_{\odot}$) at the age of the association ($\sim$4–5 Myr). The *Spitzer* sample discussed here represents 32% of all spectroscopically confirmed brown dwarf members of USco.

IRAC data for 24 of the objects were obtained on 20, 21 and 24 Aug. 2005. Exposure times were set for each source by requiring detection of photospheric emission at S/N $\sim$10 in a single pointing in all four bands (3.6, 4.5, 5.8 & 8 $\mu$m). For approximately half of the sources a 2 sec pointing was sufficient to achieve the desired S/N; for the other half a 12 sec exposure was required. All observations were taken in a five-point Gaussian pattern with medium scale factor, thus providing ample coverage for cosmic ray rejection. Three of the targets were sufficiently close to the young $\rho$ Ophucius cluster (16:25:35.12, -23:26:49.8) that they were observed serendipitously as part of the C2D Legacy program. The observing strategy for this project is given in Evans et al. (2003).

Observations using the MIPS camera in the 24 $\mu$m band were obtained in Photometry mode between Sept. 2005 and Sept. 2006. Each cycle resulted in 14 dithered exposures providing enough redundancy for cosmic ray rejection even when relatively few cycles were requested. When possible, exposure times were determined to detect *photospheric* emission with S/N $\sim$5. A maximum exposure time of 2240 seconds was imposed which was estimated to allow us the ability to detect photospheric emission

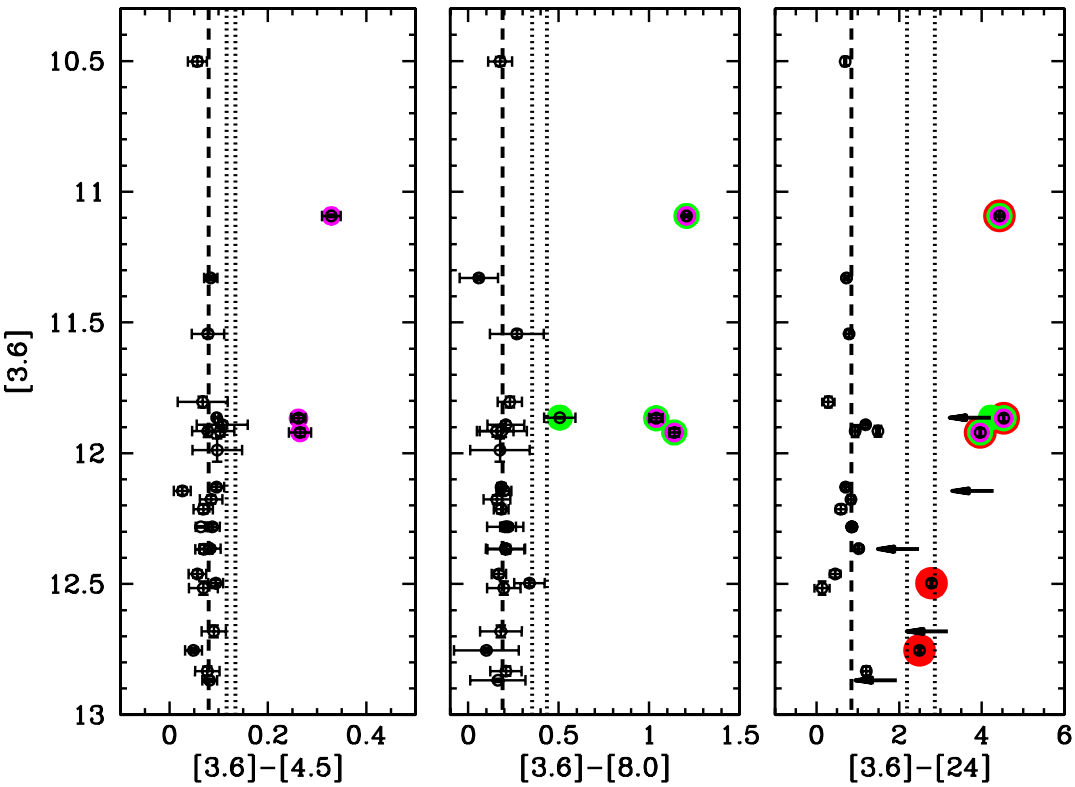


Figure 7.1 Color-magnitude diagrams for the 27 brown dwarfs observed in the *Spitzer* survey. All data have been dereddened using extinction values derived in SCH06 (chapter 5), and photometric errorbars are shown. The dashed line in each panel represents the median value of all data computed using $2\sigma$ clipping of outliers. Dotted lines represent $2\sigma$ and $3\sigma$ deviations about the median. Objects which have an excess of $> 2\sigma$ red-ward of the [3.6]-[4.5] color median are denoted with a large magenta circle in all panels. Objects which have an excess of $> 2\sigma$ red-ward of the [3.6]-[8.0] color median are denoted with a large green circle, and objects which have an excess of $> 2\sigma$ red-ward of the [3.6]-[24] color median are denoted with a large red circle. Arrows in the right panel denote five objects for which we were able only to derive upper limits at $24\mu$m.

at S/N ∼3, for even the faintest objects. However, due to highly structured, strong nebulosity present in this region, five sources were detected only as upper limits at 24$\mu$m.

Data analysis was performed on the basic calibrated data images produced by the S14 pipeline for both IRAC and MIPS. Processing of all data (including that obtained by the C2D team) was carried out primarily by my collaborator, John Carpenter, using a modified version of IDLPHOT. Details are given in Carpenter et al. (2006) and Carpenter et al. (2008, in prep.). For the IRAC data, he performed aperture photometry using a radius of 3 pixels (1".22) and a sky annulus between 10 and 20 pixels. Due to the inherently higher levels of structured background contamination at longer wavelengths, we chose to use point-spread function fitting (PSF) photometry for the MIPS data using a 5-pixel fitting radius. Photometry was calibrated to the scale given in the IRAC and MIPS manuals by applying aperture corrections of 1.109, 1.110, 1.107, 1.200, and 1.600 to the IRAC 3.6 $\mu$m, IRAC 4.5 $\mu$m, IRAC 5.8 $\mu$m, IRAC 8.0 $\mu$m, and MIPS 24 $\mu$m flux densities, respectively. Adopted photometric zeropoints were 277.52, 179.53, 116.58, 63.14, (IRAC; Reach et al. 2005) and 7.16 Jy (MIPS; Engelbracht et al. 2007). Photometry for all sources is given in table 7.1.

Figure 7.1 shows color-magnitude diagrams for the 27 brown dwarfs observed with *Spitzer*. All data have been dereddened using extinction values derived in SCH06 (and chapter 5; extinctions were derived using the reddening law by Cohen et al. 1981), and photometric errorbars are shown. The dashed line in each panel represents the median value of all data (computed using $2\sigma$ clipping of outliers), presumed to represent photospheric colors. Dotted lines represent $2\sigma$ and $3\sigma$ excess levels above the defined median photosphere. I find median photospheric colors of 0.08 mag ([3.6]-[4.5]), 0.19 mag ([3.6]-[8.0]), and 0.85 mag ([3.6]-[24]), with $1\sigma$ deviations of 2%, 8%, and 85% above photospheric levels. Objects which have an excess of $> 2\sigma$ red-ward of the color median in each panel are shown as large colored circles. Five sources represented as arrows in the right panel denote objects for which we were able only to derive upper limits at 24$\mu$m. I identify from this figure four sources which have a $> 3\sigma$ excess above the median photosphere at [3.6]-[8.0] colors. Three of these sources

Table 7.1. *Spitzer* photometry for brown dwarfs in USco

| ID | [3.6][a] | error | [4.5] | error | [5.8] | error | [8.0] | error | [24] | error[b] | $A_V$ |
|---|---|---|---|---|---|---|---|---|---|---|---|
| SCH15594802-22271650 | 12.697 | 0.023 | 12.602 | 0.008 | 12.586 | 0.068 | 12.506 | 0.113 | 9.502 | -1.000 | 0.332 |
| SCH16044303-23182620 | 12.284 | 0.011 | 12.196 | 0.009 | 12.164 | 0.057 | 12.062 | 0.042 | 11.428 | 0.095 | 0.053 |
| SCH16053077-22462016 | 12.366 | 0.011 | 12.283 | 0.018 | 12.231 | 0.028 | 12.159 | 0.107 | 11.341 | 0.088 | 0.035 |
| SCH16093018-20595409 | 12.516 | 0.011 | 12.416 | 0.009 | 12.386 | 0.081 | 12.165 | 0.083 | 9.718 | 0.016 | 0.390 |
| SCH16095991-21554293 | 12.889 | 0.006 | 12.801 | 0.013 | 12.779 | 0.085 | 12.711 | 0.152 | 10.931 | -1.000 | 0.426 |
| SCH16103876-18292353[c] | 12.008 | 0.014 | 11.716 | 0.017 | 11.411 | 0.018 | 10.812 | 0.022 | 7.985 | 0.004 | 1.780 |
| SCH16111711-22171749 | 12.833 | 0.017 | 12.756 | 0.017 | 12.733 | 0.076 | 12.624 | 0.084 | 11.626 | 0.093 | 0.000 |
| SCH16112959-19002921 | 11.965 | 0.013 | 11.835 | 0.049 | 11.802 | 0.101 | 11.709 | 0.101 | 10.722 | 0.068 | 1.517 |
| SCH16121188-20472698 | 12.141 | 0.011 | 12.042 | 0.010 | 12.023 | 0.024 | 11.951 | 0.019 | 11.428 | 0.078 | 0.235 |
| SCH16123758-23492340 | 12.485 | 0.014 | 12.421 | 0.011 | 12.367 | 0.060 | 12.300 | 0.036 | 12.013 | 0.131 | 0.480 |
| SCH16124692-23384086 | 12.228 | 0.016 | 12.155 | 0.010 | 12.115 | 0.042 | 12.036 | 0.037 | 11.626 | 0.123 | 0.290 |
| SCH16131212-23050329 | 12.516 | 0.025 | 12.447 | 0.013 | 12.392 | 0.034 | 12.319 | 0.089 | 12.379 | 0.179 | 0.000 |
| SCH16141974-24284053 | 12.308 | 0.003 | 12.236 | 0.010 | 12.207 | 0.033 | 12.086 | 0.100 | 11.428 | 0.070 | 0.544 |
| SCH16151115-24201556 | 12.774 | 0.009 | 12.719 | 0.013 | 12.636 | 0.075 | 12.660 | 0.178 | 10.266 | 0.024 | 0.417 |
| SCH16155508-24443677 | 11.828 | 0.020 | 11.753 | 0.046 | 11.731 | 0.084 | 11.582 | 0.063 | 11.523 | 0.147 | 0.490 |
| SCH16174540-23533618 | 12.429 | 0.016 | 12.340 | 0.005 | 12.312 | 0.076 | 12.180 | 0.100 | 9.904 | -1.000 | 1.262 |
| SCH16200756-23591522 | 11.601 | 0.014 | 11.505 | 0.029 | 11.355 | 0.033 | 11.294 | 0.147 | 10.770 | 0.085 | 1.180 |
| SCH16202127-21202923 | 11.935 | 0.020 | 11.826 | 0.019 | 11.764 | 0.143 | 11.765 | 0.091 | 10.433 | 0.039 | 0.408 |
| SCH16213591-23550341 | 12.212 | 0.014 | 12.165 | 0.009 | 12.131 | 0.009 | 11.970 | 0.037 | 7.880 | -1.000 | 1.380 |
| SCH16224384-19510575 | 10.538 | 0.017 | 10.470 | 0.009 | 10.450 | 0.065 | 10.338 | 0.063 | 9.815 | 0.008 | 0.748 |
| SCH16235158-23172740[c] | 11.864 | 0.002 | 11.768 | 0.003 | 11.650 | 0.112 | 11.358 | 0.086 | 7.646 | -1.000 | 0.000 |
| SCH16235474-24383211 | 11.431 | 0.009 | 11.316 | 0.009 | 11.291 | 0.009 | 11.306 | 0.105 | 10.631 | 0.063 | 2.071 |
| SCH16252862-16585055 | 12.178 | 0.015 | 12.093 | 0.016 | 12.056 | 0.027 | 12.018 | 0.072 | 11.341 | 0.072 | 0.021 |
| SCH16253671-22242887 | 11.948 | 0.023 | 11.860 | 0.022 | 11.862 | 0.105 | 11.740 | 0.136 | 10.988 | 0.064 | 0.665 |
| SCH16263026-23365552[c] | 11.240 | 0.004 | 10.866 | 0.018 | 10.585 | 0.055 | 9.937 | 0.011 | 6.706 | 0.002 | 3.017 |
| SCH16265619-22135224 | 12.007 | 0.044 | 11.904 | 0.024 | 11.864 | 0.136 | 11.819 | 0.158 | 0.000 | 0.000 | 0.390 |
| SCH16324726-20593771[c] | 11.869 | 0.013 | 11.606 | 0.005 | 11.343 | 0.031 | 10.828 | 0.034 | 7.336 | 0.003 | 0.062 |

[a]All photometry given in magnitudes with associated error.

[b]An error on MIPS 24$\mu$m photometry of -1.000 indicates the magnitude given is a 3$\sigma$ upper limit.

[c]This brown dwarf has a [3.6]-[8.0] color excess as defined in §7.2.

have a confirmed $> 3\sigma$ excess at [3.6]-[24] colors. The fourth may also have a [3.6]-[24] excess; however, it was detected only as an upper limit at 24 $\mu$m. Two additional sources exhibit an excess at [3.6]-[24] color at the $> 2\sigma$ level. These stars do not have a [3.6]-[8.0] color excess and *may* represent disks that have begun to clear material from the inside out; however, without data at longer wavelengths I cannot draw any definitive conclusions. The four brown dwarfs with [3.6]-[8.0] color excess emission at $> 3\sigma$ levels (i.e., $\gtrsim$25% above photospheric levels) are listed as excess sources in table 7.1. I note at this time that the RMS residual about the median [3.6]-[8.0] color, $\sim$8.3%, is slightly *lower* than the average $([3.6]\text{-}[8.0])_{error}$, $\sim$8.6%. Thus, the photometric uncertainties given in table 7.1 are likely overestimated.

Because the *Spitzer* observations began before the spectroscopic follow-up program in USco was complete, only one of the five brown dwarfs (spectral type$\geq$M6) determined in §5.3.3 to be accreting was included in the *Spitzer* target list. That source, SCH16103876-18292353, does have mid-infrared excess emission above photospheric colors at all IRAC and MIPS wavelengths (see table 7.1). SCH16235158-23172740, the M8-type brown dwarf that exhibited the strongest H$\alpha$ emission, significantly above the accretor/nonaccretor division defined by Barrado y Navascués & Martín (2003), is also observed to have a mid-infrared excess.

## 7.3 The Evolution of Circumstellar Disks with Mass

In order to place my results into context, I have compared my data to those for 1) similar age stars at higher masses, and 2) similar mass brown dwarfs at different ages. To allow robust conclusions to be drawn, I have re-derived the disk frequency for my sample in §7.3 and §7.4 using criteria which takes into account both my data and the appropriate comparison sample. Thus, differences in computed disk frequencies between §7.2, §7.3, and §7.4 reflect changes in the criteria adopted to define a source with a mid-infrared excess, *not* changes in the data.

Figure 7.2 shows a 2MASS-IRAC color-color diagram for the sample of brown dwarfs presented here (circles) together with observations from Carpenter et al. (2006)

for higher mass stellar members of USco with spectral types B–M5 (triangles). The red solid line indicates a linear fit to the data, computed with $3\sigma$ clipping of outliers and presumed to represent photospheric colors. RMS residuals of the fit are dominanted by small uncertainties measured for the stellar photometry; thus, the limiting uncertainties are not fit residuals but the photometric uncertainties of the low mass brown dwarfs. I therefore adopt a threshold to define an excess source corresponding to 3× the average $([4.5]\text{-}[8.0])_{error}$ for the brown dwarfs, or ∼24% above photospheric colors. The four brown dwarfs with a [3.6]-[8.0] color excess also have an excess at [4.5]-[8.0] colors, and exhibit similar [4.5]-[8.0] colors to those computed for K- and M-type stars with disks identified by Carpenter et al. (2006). Based on the adopted criteria listed above to identify infrared excess sources, the disk frequency for M stars (M0–M5) in the study by Carpenter et al. (2006) is 16/101 ($\sim 16^{+5}_{-4}\%$). I measure a disk frequency for brown dwarfs of $15^{+12}_{-7}\%$. Using a two-tailed Fisher's Exact test, these frequencies are indistinguishable from each other implying a near-constant frequency in USco of stars with disks compared to stars without disks spanning a mass range from ∼0.5 $M_\odot$ to ∼0.02 $M_\odot$. Thus, the observations I presented here add to the growing evidence that substellar formation and early evolution must proceed through very similar physical processes as those that form and shape low mass stars.

The measured disk frequency for my sample is lower than the value of 37±9% (measured using different criteria — see below) reported by Scholz et al. (2007) for substellar members of USco. This study took MIPS 24$\mu$m photometry and 8–12$\mu$m IRS spectroscopy of 35 brown dwarfs in USco that had been identified in the literature prior to my Quest-2 surveys. The reason for the discrepancy in measured disk frequencies is not obvious. However, one difference between our two works is that Scholz et al. (2007) used $K$-[24] colors to identify sources with excess emission at 4× the photospheric value calculated from theoretical blackbody colors, whereas I have used empirical IRAC colors. In order to assess the significance of the difference between our two results, I have recomputed the disk frequency for both data sets adopting consistent criterion to identify sources with infrared excess emission. In figure 7.3 I show the 2MASS $K_S$ vs. $K_S$-[24] color magnitude diagram for the 27 brown dwarfs

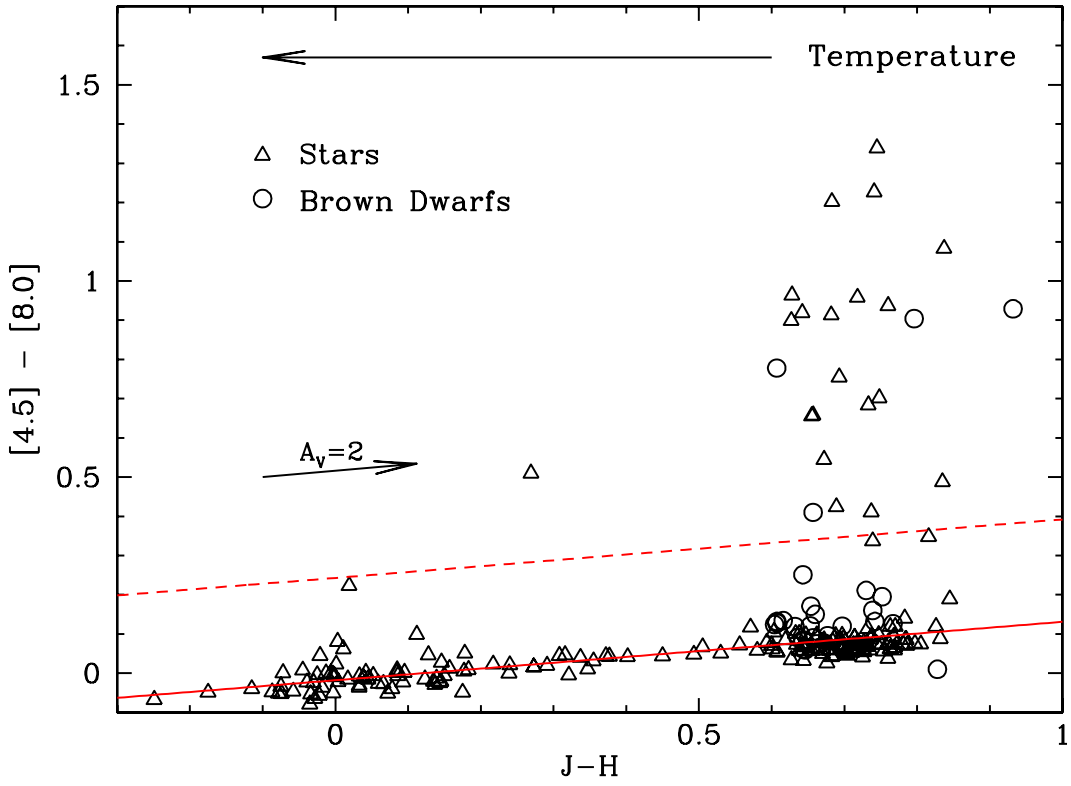


Figure 7.2 $J - H$ vs. [4.5]-[8.0] color-color diagram for substellar (circles; presented here) and stellar (triangles; taken from Carpenter et al. 2006) members of USco. Solid line indicates a linear fit to the data and dashed line indicates the threshold adopted to identify excess sources corresponding to a color excess of 24% above the photosphere.

in my USco survey (black), together with data from Scholz et al. (2007). I have included only the 27 brown dwarfs from the Scholz et al. (2007) work with spectral types M6–M8, so as to compare a consistent samples. Black and red triangles represent upper limits. Note that Scholz et al. (2007) report the *survey* upper limit, but not the upper limit for individual sources. Thus, I have used the survey upper limit in each case causing the linear line of red triangles. As in figure 7.1, the dashed line represents the median value of all data in my sample (computed using $2\sigma$ clipping of outliers), presumed to represent photospheric colors. Dotted lines represent $2\sigma$ and $3\sigma$ deviations about the median. As can be seen, using this criteria I do not identify any additional sources (beyond the four identified in §7.2) with measured $K_S$-[24] in excess of $3\sigma$ ($\sim$500%) above the photospheric color ($K_S$-[24]=1.34 mag), and actually measure a lower disk frequency of $3/27 = 11^{+11}_{-6}$%. Adopting the same criterion to calculate the disk frequency from the Scholz et al. (2007) dataset, I measure a disk frequency of $8/27 = 30^{+14}_{-11}$%. Thus, the two results are consistent, but only at the $1\sigma$ level.

## 7.4 The Evolution of Circumstellar Disks with Age

The second method by which I can place into context the results from my mid-infrared study of 5 Myr-old brown dwarfs in USco, is to analyze them in comparison to results from similar observations of brown dwarfs at different ages. Mid-infrared *Spitzer* observations have been carried out for several other nearby associations, including IC 348 (3 Myr, 320 pc; Lada et al. 2006, Luhman et al. 2005), Chameleon I (2 Myr, 165 pc; Luhman et al. 2005), and the young Taurus subclusters (1 Myr, 140 pc; Hartmann et al. 2005, Luhman et al. 2006, Guieu et al. 2007). I have compiled measured IRAC photometry for brown dwarfs in these associations from three of the studies that extended to substellar masses (Luhman et al. 2006, Lada et al. 2006, Luhman et al. 2005), together with extinctions and/or spectral types from Luhman (2004a) (Chameleon I), Luhman et al. (2003b) (IC 348), and Briceño et al. (2002), Luhman et al. (2003a), Guieu et al. (2006) (Taurus). I limited my literature search

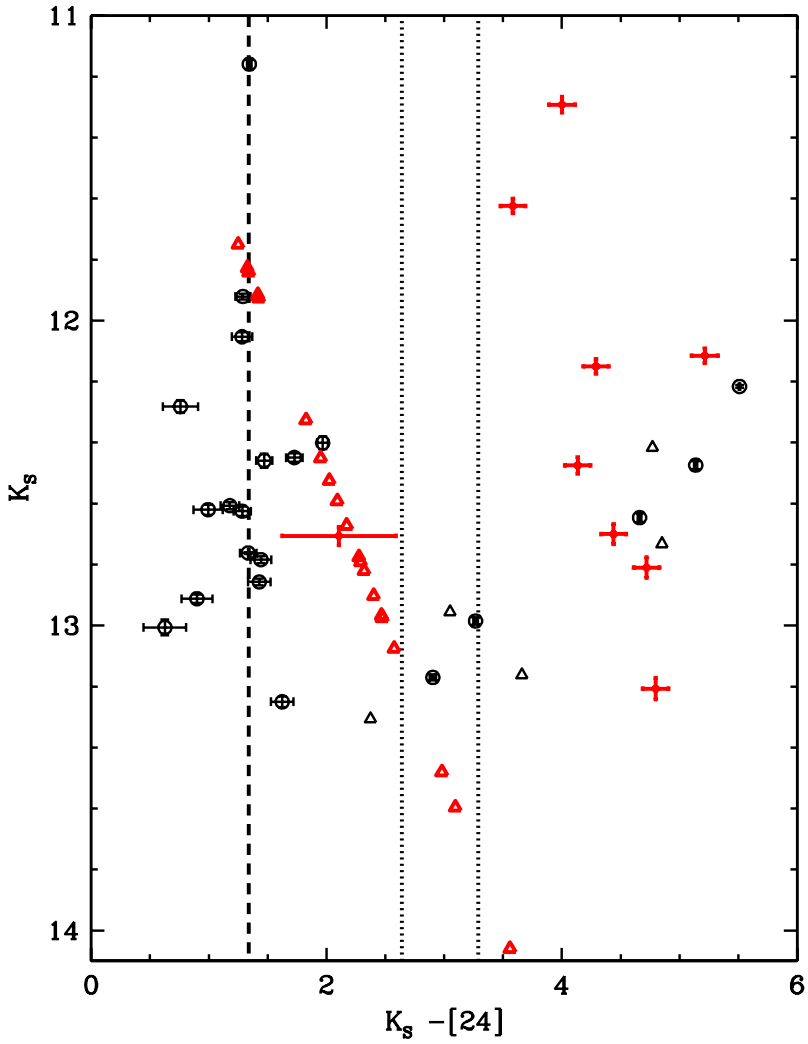


Figure 7.3 2MASS $K_S$ vs $K_S$-[24] color magnitude diagram for the 27 brown dwarfs in my USco survey (black), together with data for M6-M8 brown dwarfs from Scholz et al. (2007) (red). Black and red triangles represent upper limits. Dashed and dotted lines are as defined in figure 7.1.

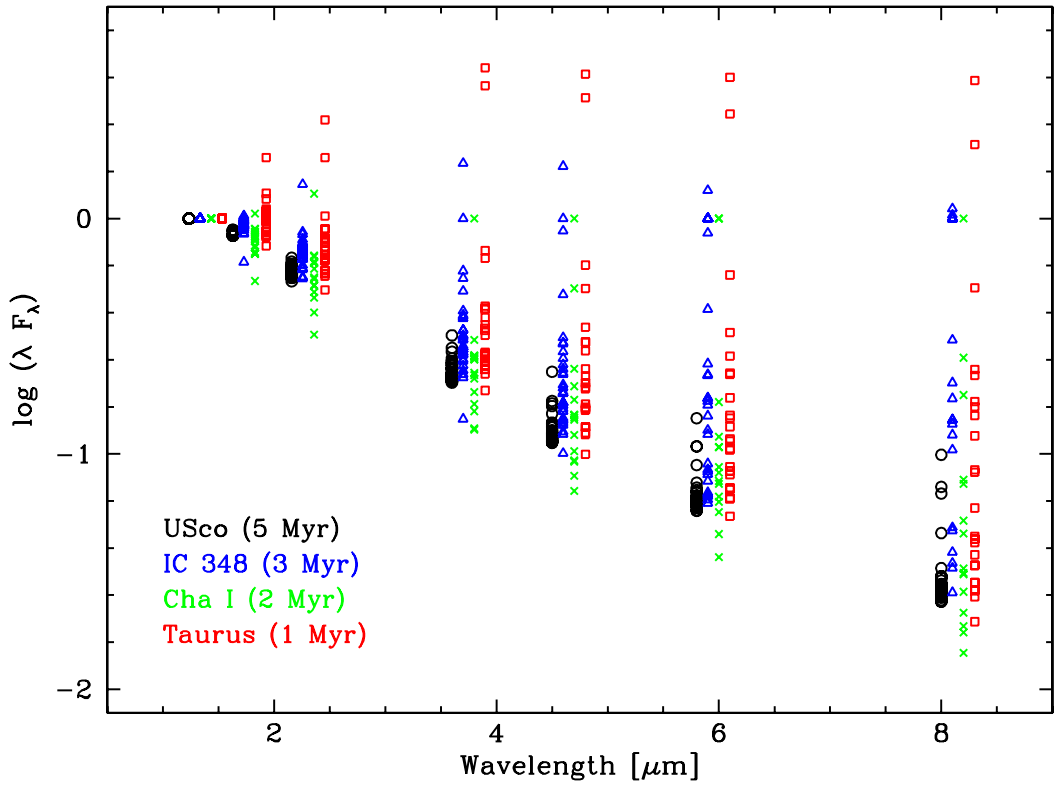


Figure 7.4 Dereddened SEDs for brown dwarfs with spectral types M6–M8 from 1 to 5 Myr. Data for IC 348 (3 Myr; blue), Chameleon I (2 Myr; green), and Taurus (1 Myr; red) are taken from the literature (see text). All stars have been normalized to unity at $J$-band and an offset has been applied to the wavelength data for stars in associations other than USco for ease of comparison.

to include only those brown dwarfs in the surveys listed above with spectral types M6-M8, thus providing samples analogous to the one presented here for USco. In total, I find 25 brown dwarfs in Taurus, 12 in Chameleon I, and 24 in IC 348 to have measured IRAC photometry and spectral types M6-M8.

In figure 7.4 I show dereddened spectral energy distributions (SEDs) for these brown dwarfs together with SEDs for the brown dwarfs observed in USco. Flux for all objects has been normalized to unity at J-band. As can be seen, the SEDs for the brown dwarfs in USco (black) that exhibit an [8.0] excess have systematically lower flux than the brown dwarfs with an excess in the three younger clusters or associations. In figure 7.5 I have computed the percentage of objects with a [3.6]-

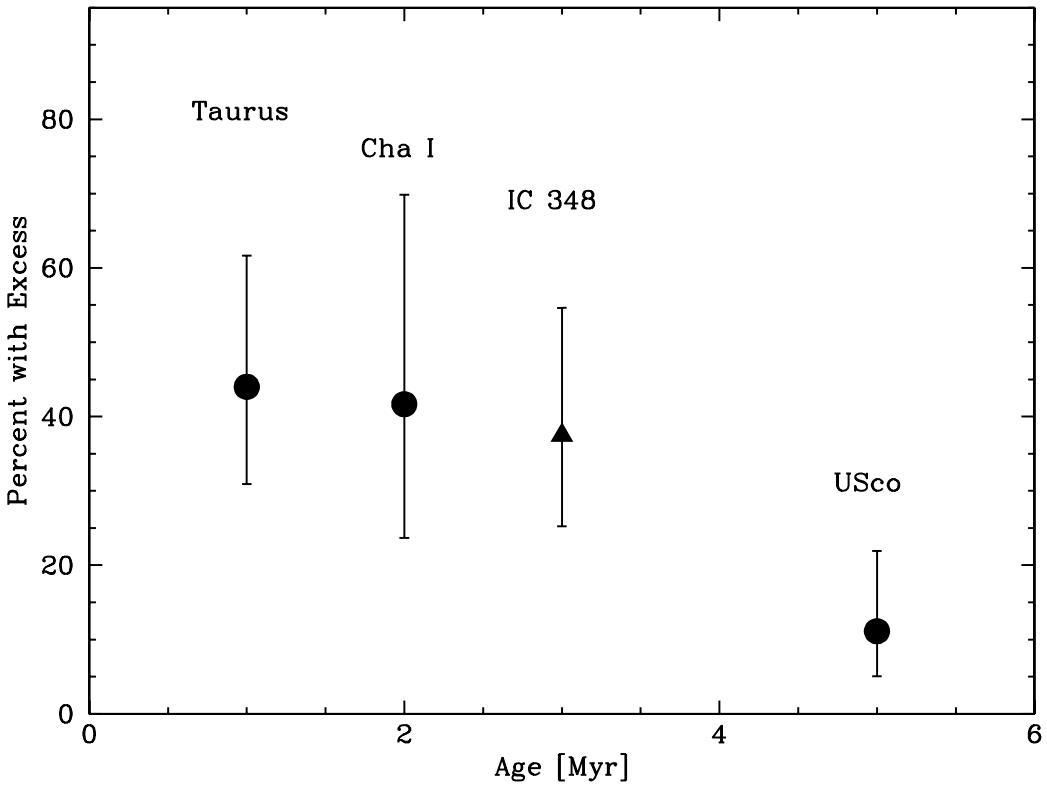


Figure 7.5 Percentage of brown dwarfs in the USco and comparison samples (see text) as a function of mean cluster age. IC 348 is shown as a triangle because only 14/24 brown dwarfs were detected at 8$\mu$m in the Lada et al. (2006) survey. Thus, the value shown is a lower limit.

[8.0] color excess using the same method that I used to define an excess source in USco. Median photometric uncertainties for the three comparison samples are 0.058 mag (Taurus), 0.036 mag (Chameleon I), and 0.16 mag (IC 348). Thus, the limiting uncertainty is that for the IC 348 stars. Therefore, for the purpose of this comparison, I take $1\sigma$=0.16 and define a source to have an excess if it has [3.6]-[8.0] colors >56% (i.e., $>3\sigma$) above the photospheric level of 0.19 mag. The disk frequency for IC 348 is shown in figure 7.5 as a triangle because only 14/24 brown dwarfs were detected at 8$\mu$m in the Lada et al. (2006) survey. Thus, the value shown is a lower limit. I find disk frequencies of $44^{+18}_{-14}$% (11/25) for Taurus, $42^{+28}_{-18}$% (5/12) for Chameleon I, and $38^{+17}_{-12}$% (9/24) for IC 348. While the measured disk frequencies do decline with increasing age from 1 to 3 Myr for these regions, considering the large associated errors, these values are statistically indistinguishable from each other. Thus, to increase the size of the sample analyzed, I combine data for the three associations younger than ∼3 Myr and derive a disk frequency of $41^{+10}_{-9}$% (25/61). For my sample of brown dwarfs in USco I measure a disk frequency of $11^{+11}_{-6}$% (3/27) (one source did not have a large enough excess to be considered to exhibit a mid-infrared excess when I used the larger sigma cutoff). Using a two-tailed Fisher's Exact test I find the disk frequencies for the associations younger than ∼3 Myr to be different from that for the 5 Myr-old brown dwarfs in USco with ∼94% confidence.

Based on results of comparison between these four star forming regions, I infer that about half of brown dwarfs clear the inner regions of their circumstellar material within the first ∼1 Myr (i.e., by an age of Taurus). The other half do not begin to dissipate circumstellar material until ∼3 Myr, but then this process must proceed rapidly for most objects through ∼5 Myr. One caveat to this argument which must be mentioned is that Taurus, IC 348, Chameleon I, and USco all represent different environments. As discussed in previous chapters, Taurus is an example of an isolated, low density star forming region whereas USco is a large OB association. Neither IC 348 nor Chameleon I contain stars hot enough to ionize material; however, they are much more dense star-forming environments than either Taurus or USco. Thus, until we have a better understanding of the role environment may play in circumstellar disk

lifetime, we cannot draw definitive conclusions about the rate at which circumstellar evolution proceeds around the lowest mass stars and brown dwarfs.

## 7.5 Summary and Conclusions

I have observed 27 brown dwarfs identified as part of my thesis work using the IRAC and MIPS mid-infrared cameras on the *Spitzer Space Telescope*. From these data I have identified four brown dwarfs ($15^{+12}_{-7}$%) that possess an infrared excess. Based on comparison with work by Carpenter et al. (2006) of higher mass association members, I find the disk frequency in USco to be near-constant for M-type objects from $M$ ∼0.5 to 0.02 $M_{\odot}$. I have also compared my results for 5 Myr-old brown dwarfs in USco to those for 1,2, and 3 Myr-old brown dwarfs at similar masses in the young Taurus subclusters, and the star forming regions of Chameleon I and IC 348. I measure a disk frequency of ∼40% for brown dwarfs from 1–3 Myr, declining sharply by the age of USco (5 Myr). Thus, assuming environmental factors do not play a large role in the lifetimes of disks around the lowest mass stars and brown dwarfs (which does not have to be true!), the evolution of circumstellar material must proceed rapidly around such objects between 3 and 5 Myr. Larger samples spanning a range of both environment and age are needed to confirm this result.